AIAA JOURNAL
Vol. 34, No. 2, February 1996

Suppression of Nonlinear Panel Flutter at Supersonic Speeds and Elevated Temperatures

R. C. Zhou,* Chuh Mei,† and Jen-Kuang Huang‡
Old Dominion University, Norfolk, Virginia 23529-0247

Coupled structure-electrical nonlinear panel flutter equations of motion are derived using the finite element method for composite panels with embedded piezoelectric layers subjected to thermal loads. The von Kármán large-deflection strain-displacement relations, quasisteady first-order piston theory aerodynamics, quasisteady thermal stress theory, and linear piezoelectricity theory are used. Following a modal transformation and reduction, a set of coupled nonlinear modal equations of motion is obtained. By using the linear optimal control design for the linearized modal equations, an optimal shape and location of piezoelectric actuators can be determined. Numerical simulations based on the nonlinear modal equations show that the maximum flutter-free dynamic pressure with the linear optimal control can be increased as high as six times of the critical dynamic pressure. The panel's large-amplitude limit-cycle motions, as well as periodic and chaotic motions at moderate temperatures, are shown to be completely suppressed within the maximum flutter-free dynamic pressure region. Flutter suppression on composite panels with different aspect ratios, boundary conditions, and thermal effects are also studied. The results reveal that piezoelectric actuators are effective in nonlinear panel flutter suppression.

Nomenclature

$[A], [B], [D]$	= extension, coupling, and bending panel stiffness matrices
$[A_a], [a_a]$	= system and element aerodynamic influence matrices
a, b	= panel length and width
$\boldsymbol{C}_d$	= modal aerodynamic damping matrix
c_a	= air-panel mass ratio over Mach number
D_3, E_3	= electric displacement and field
$\{d\}$	= electromechanical coefficients
$\boldsymbol{F}$	= modal force vector
$[G], [g]$	= system and element aerodynamic damping matrices
g_a	= nondimensional aerodynamic damping
h_p, h	= thickness of piezoelectric layer and panel
$\boldsymbol{K}$	= modal stiffness matrix
$[K], [k]$	= system and element linear stiffness matrices
$[K1], [k1]$	= first-order nonlinear stiffness matrices
$[K2], [k2]$	= second-order nonlinear stiffness matrices
$\boldsymbol{k}$	= feedback control gain matrix
$\boldsymbol{M}$	= modal mass matrix
$[M], [m]$	= system and element mass matrices
M_∞	= Mach number
$\{P\}, \{p\}$	= system and element load vectors
p_a	= aerodynamic pressure
$\boldsymbol{Q}, \boldsymbol{R}$	= penalty matrices
$\boldsymbol{q}$	= modal amplitude vector
q_a	= dynamic pressure
t	= time
u, v, w	= displacement
$\{W\}, \{w\}$	= system and element nodal displacement vectors
$\boldsymbol{X}$	= state space vector
x_s	= width of piezoelectric material placed at the leading edge
$\{\alpha\}$	= thermal expansion coefficients
ΔT	= temperature change
ε, γ	= strain components
$[\Theta]_l, [\Theta]_{nl}$	= linear and nonlinear electromechanical coupling matrices
$\{\kappa\}$	= curvature vector
λ	= nondimensional dynamic pressure
μ	= air-panel mass ratio
ρ	= density
σ, τ	= stress components
Ψ, φ	= modal matrix and normal mode
ω_0	= reference frequency

Subscripts

a	= air
b	= bending
cr	= critical
m	= membrane
ΔT	= thermal
θ	= nonlinear
ϕ	= electrical

Introduction

PANEL flutter is a self-excited, dynamic instability of thin plate or shell-like structural components of flight vehicles. It is a supersonic/hypersonic aeroelastic phenomenon that is often encountered in the operation of aircraft and missiles. The airflow is only on one side of the panel. Because of the large-deflection geometrical structural nonlinearity, limit-cycle oscillations will occur beyond the critical dynamic pressure. When a flight vehicle travels at high supersonic speeds, it not only will experience flutter due to the dynamic pressure but also will be affected by increased temperature owing to the aerodynamic heating. The presence of high temperature load results in a flutter motion at lower dynamic pressures. In addition, the temperature rise may also cause large aerodynamic-thermal deflections of the skin panels, which affects flutter response and can lead to chaotic motion. The mode of failure for panel flutter is fatigue due to limit-cycle oscillations. To increase the critical dynamic pressure or to suppress the limit-cycle oscillations is, therefore, one of the many important factors that a designer should consider. Conventional design is to increase the panel stiffness, which, in turn, may result in additional weight. With the development of high-speed

Presented as Paper 94-1743 at the AIAA/ASME 35th Adaptive Structures Forum, Hilton Head, SC, April 18–22, 1994; received Jan. 30, 1995; revision received Sept. 13, 1995; accepted for publication Sept. 15, 1995.

*Ph.D. Student, Department of Aerospace Engineering; currently Engineer, Mechanical Design Sort Facilities Development, FedEx Corp., Memphis, TN 38194. Student Member AIAA.

†Professor, Department of Aerospace Engineering. Associate Fellow AIAA.

‡Associate Professor, Department of Mechanical Engineering. Senior Member AIAA.

flight vehicles such as the high-speed civil transport (HSCT), the National Aerospace Plane (NASP), and the YF-22 Advanced Tactical Fighter (ATF), panel flutter thus becomes one of the important issues to be considered.

An earlier and excellent survey article on linear and nonlinear panel flutter through 1970 was given by Dowell.[1] Flutter of simply supported isotropic panels[2] was investigated using first-order quasisteady piston theory.[3] The analytical limit-cycle results agreed well with the wind-tunnel testing data.[1] Gray and Mei[4] conducted a complete survey on various theoretical considerations and analytical methods for the investigation of nonlinear panel flutter up to 1991. Most recently, Zhou et al.[5] conducted a survey on various approaches, including finite element methods, on nonlinear panel flutter analysis.

Many researchers have investigated the effectiveness of using smart materials for passive or active control of flexible structures. Only a few research papers have been reported in the area of control of panel flutter response using adaptive materials. Scott and Weisshaar[6] were the first to study controlling linear panel flutter using piezoelectric materials. Only four modes in the x direction (one in y direction) were retained in the study using the Ritz method. Hajela and Glowasky[7] applied piezoelectric elements in supersonic linear panel flutter suppression. Finite element models for panels with surface bonded and embedded piezoelectric materials were created to determine the response. The optimal panel configuration with minimum weight and optimal sizing and layout of piezoelectric elements for maximum flutter dynamic pressure were determined by a multicriterion optimization scheme. In both studies,[6,7] the bending moment induced by the piezoelectric materials is not effective in controlling linear panel flutter since there is no bending behavior in the linear case. On the other hand, the induced in-plane force is not sufficient in panel flutter control because of the low modulus and limited ability of the piezoelectric materials to create large panel in-plane stress. Lai et al.[8] studied to control the nonlinear flutter of a simply supported isotropic plate by using piezoelectric actuators. The Galerkin's approach was adopted in obtaining the nonlinear modal equations of motion. They concluded that the bending moment was effective in flutter suppression. Xue and Mei[9] recently studied the feasibility of the application of shape memory alloy (SMA) in linear panel flutter control. The finite element equations of motion were developed for panel flutter including thermal and SMA effects. The results showed that the SMA was effective in passive control of panel flutter at high temperatures. Zhou et al.[10] employed the finite element method to the nonlinear flutter suppression of isotropic panels with surface bonded piezoelectric materials.

In this paper, a coupled structural and electrical finite element formulation is presented for suppression of nonlinear flutter motions of composite panels at supersonic speeds and elevated temperatures ($\Delta T/\Delta T_{cr} > 1$, but within the piezoelectric material Curie's point). The nonlinear finite element equations of motion, based on von Kármán's large-deflection theory, are developed for composite panels with embedded piezoelectric layers subjected to aerodynamic and thermal loads. A modal transformation and reduction is then performed to obtain a set of equations of motion in modal coordinates. The norm of feedback control gain (NFCG) based on the optimal control method is employed to determine the shape and location of the embedded actuators. Beacuse of the limitation of the maximum operating electric field of the piezoelectric actuator (set at one-half of depolarization in this study), there is a maximum dynamic pressure beyond which the flutter motion can no longer be suppressed. It is referred to as the maximum flutter-free dynamic pressure λ_{max}. Numerical simulations based on the nonlinear modal equations are performed to demonstrate the effectiveness of panel flutter suppression under the piezoelectric actuation. The maximum flutter-free dynamic pressure is investigated and presented for composite panels of different stacking sequences, aspect ratios, and support conditions at ambient and elevated temperatures.

Finite Element Formulation

First-Order Piston Theory Aerodynamics

For panel flutter at high supersonic flow, the quasisteady first-order piston theory[1-5] is usually employed. The aerodynamic load can be expressed as

$$p_a = -\frac{2q_a}{\beta}\left[\frac{\partial w}{\partial x} + \left(\frac{M_\infty^2 - 2}{M_\infty^2 - 1}\right)\frac{1}{V_\infty}\frac{\partial w}{\partial t}\right]$$

$$= -\left(\lambda\frac{D_{110}}{a^3}\frac{\partial w}{\partial x} + \frac{g_a}{\omega_0}\frac{D_{110}}{a^4}\frac{\partial w}{\partial t}\right) \tag{1}$$

where $q_a = \rho_a V_\infty^2/2$ is the dynamic pressure, ρ_a the air mass density, V_∞ the freestream airflow speed, $\beta = (M_\infty^2 - 1)^{1/2}$, and D_{110} the first entry of the laminate bending stiffness matrix calculated when all of the fibers of the composite layers are aligned in the direction of the airflow (x direction). The nondimensional dynamic pressure and aerodynamic damping are given by

$$\lambda = \frac{2q_a a^3}{\beta D_{110}}, \qquad g_a = \frac{\rho_a V_\infty (M_\infty^2 - 2)}{\rho h \omega_0 \beta^3} \tag{2}$$

where ρ is the average mass density of the panel, h the panel thickness, and $\omega_0 = (D_{110}/\rho h a^4)^{1/2}$ is a convenient reference frequency. Other commonly used nondimensional parameters are the air-panel mass ratio and aerodynamic damping coefficient, which are defined as

$$\mu = \frac{\rho_a a}{\rho h}, \qquad c_a = \left(\frac{M_\infty^2 - 2}{M_\infty^2 - 1}\right)^2 \frac{\mu}{\beta} \tag{3}$$

From Eqs. (2) and (3), $g_a = \sqrt{(\lambda c_a)}$ and $c_a \approx \mu/M_\infty$ for $M_\infty \gg 1$.

Modified Rectangular Plate Element

The plate bending element employed in the present study is the C^1 conforming rectangular element with an additional electrical potential at the center of each piezoelectric layer. The 16 element bending and the 8 in-plane nodal displacements at the four vertices are

$$\{w_b\} = \{w_1, w_2, w_3, w_4, w_{x1}, w_{x2}, w_{x3}, w_{x4}, w_{y1}$$

$$w_{y2}, w_{y3}, w_{y4}, w_{xy1}, w_{xy2}, w_{xy3}, w_{xy4}\}^t \tag{4}$$

$$\{w_m\} = \{u_1, u_2, u_3, u_4, v_1, v_2, v_3, v_4\}^t \tag{5}$$

The electrical degree of freedom is assumed to be constant throughout the plane of each piezoelectric layer and to vary linearly through the thickness. The electrical degrees of freedom can thus be written as

$$\{w_\phi\} = \{V_1, V_2, \ldots, V_{np}\}^t \tag{6}$$

where V_i are the electrical potentials applied or detected in the center of each piezoelectric layer, and np denotes the number of piezoelectric layers.

Constitutive Equations

In the derivation of equations of motion, it is assumed that the panel is thin; i.e., the ratio of length or width over thickness of the panel is greater than 50. The rotary inertia and transverse shear deformation effects are thus negligible. The von Kármán nonlinear strain-displacement relationships are given by

$$\{\varepsilon\} = \begin{Bmatrix} u_{,x} \\ v_{,y} \\ u_{,y} + v_{,x} \end{Bmatrix} + \frac{1}{2}\begin{Bmatrix} w_{,x}^2 \\ w_{,y}^2 \\ 2w_{,x}w_{,y} \end{Bmatrix}$$

$$- z\begin{Bmatrix} w_{,xx} \\ w_{,yy} \\ 2w_{,xy} \end{Bmatrix} = \{\varepsilon_m^0\} + \{\varepsilon_\theta^0\} + z\{\kappa\} \tag{7}$$

where u and v are the in-plane displacements. The membrane strains $\{\varepsilon_m^0\}$ and $\{\varepsilon_\theta^0\}$ are due to in-plane displacements and large deflections, respectively.

For an aircraft panel consisting of fiber-reinforced composite layers and piezoelectric layers subjected to a temperature change of $\Delta T(x, y, z)$, the stress-strain relationships for a general kth layer, either the fiber-reinforced composite (set $E_{3k} = 0$) or the piezoelectric layer, can be expressed as[11,12]

$$\begin{Bmatrix} \sigma_x \\ \sigma_y \\ \tau_{xy} \end{Bmatrix}_k = \begin{bmatrix} \bar{Q}_{11} & \bar{Q}_{12} & \bar{Q}_{16} \\ \bar{Q}_{12} & \bar{Q}_{22} & \bar{Q}_{26} \\ \bar{Q}_{16} & \bar{Q}_{26} & \bar{Q}_{66} \end{bmatrix}_k \left\{ \begin{Bmatrix} \varepsilon_x \\ \varepsilon_y \\ \gamma_{xy} \end{Bmatrix} - \Delta T \begin{Bmatrix} \alpha_x \\ \alpha_y \\ \alpha_{xy} \end{Bmatrix}_k - E_{3k} \begin{Bmatrix} d_x \\ d_y \\ d_{xy} \end{Bmatrix}_k \right\} \tag{8a}$$

For piezoelectric layers, the corresponding electric displacements are only detected along the poling axis. The electric displacement for the kth layer can be expressed as

$$D_{3k} = \begin{bmatrix} d_x & d_y & d_{xy} \end{bmatrix}_k \begin{bmatrix} \bar{Q}_{11} & \bar{Q}_{12} & \bar{Q}_{16} \\ \bar{Q}_{12} & \bar{Q}_{22} & \bar{Q}_{26} \\ \bar{Q}_{16} & \bar{Q}_{26} & \bar{Q}_{66} \end{bmatrix}_k \times \begin{Bmatrix} \varepsilon_x \\ \varepsilon_y \\ \gamma_{xy} \end{Bmatrix} + \left(\epsilon_{33}^{\varepsilon}\right)_k E_{3k} \tag{8b}$$

where $[\bar{Q}]_k$ is the transformed reduced lamina stiffness matrix.

The stress resultants, per unit length, are defined as

$$(\{N\}, \{M\}) = \int_{-h/2}^{h/2} \{\sigma\}_k (1, z)\, \mathrm{d}z \tag{9}$$

which lead to the constitutive relations for a laminated panel:

$$\begin{Bmatrix} N \\ M \end{Bmatrix} = \begin{Bmatrix} A & B \\ B & D \end{Bmatrix} \begin{Bmatrix} \varepsilon^0 \\ \kappa \end{Bmatrix} - \begin{Bmatrix} N_{\Delta T} \\ M_{\Delta T} \end{Bmatrix} - \begin{Bmatrix} N_e \\ M_e \end{Bmatrix} \tag{10}$$

The laminate stiffness matrices are given by

$$([A], [B], [D]) = \int_{-h/2}^{h/2} [\bar{Q}]_k (1, z, z^2)\, \mathrm{d}z \tag{11}$$

Equations of Motion

In the derivation of the finite element equations of motion for the laminated composite panel with piezoelectrically coupled electromechanical properties, the generalized Hamilton principle is adopted from Crandall et al.[11]:

$$\int_{t_1}^{t_2} \delta(T - U + W_e - W_m + W)\, \mathrm{d}t = 0 \tag{12}$$

where T and U are kinetic energy and strain energy of the system, W_e is electrical energy, W_m is magnetic energy, and W is the work done due to external forces and the applied surface charge only. For piezoceramics the magnetic term W_m is negligible. By evaluating the energy terms in Eq. (12) with the consideration of piezoelectric and thermal effects, one can simply obtain the variational equation as

$$\int_{\forall} [\rho(\{\delta\dot{w}\}^t\{\dot{w}\} + \{\delta\dot{u}\}^t\{\dot{u}\} + \{\delta\dot{v}\}^t\{\dot{v}\}) - \{\delta\varepsilon\}^t\{\sigma\} + \{\delta E\}^t\{D\} + \{\delta w\}^t\{F_b\}\, \mathrm{d}\forall + \int_{S_1} \{\delta w\}^t\{F_s\}\, \mathrm{d}S - \int_{S_2} \delta V \sigma'\, \mathrm{d}S + \{\delta w\}^t\{F_c\} = 0 \tag{13}$$

where $\{F_b\}$ is the body force, $\{F_s\}$ is the surface traction, $\{F_c\}$ is the concentrated load, S_i is the surface area, and σ' is the surface charge.

The volume integral can be reduced to the area integral by first integrating the integrands along the thickness direction and then applying the constitutive equations. With the use of finite element expressions, the equations of motion for a rectangular plate element subjected to a dynamic pressure, temperature change, and electric field with aerodynamic damping are obtained and can be expressed as

$$\frac{1}{\omega_0^2}\begin{bmatrix} m_b & 0 & 0 \\ 0 & m_m & 0 \\ 0 & 0 & 0 \end{bmatrix}\begin{Bmatrix} \ddot{w}_b \\ \ddot{w}_m \\ \ddot{w}_\phi \end{Bmatrix} + \frac{g_a}{\omega_0}\begin{bmatrix} g & 0 & 0 \\ 0 & 0 & 0 \\ 0 & 0 & 0 \end{bmatrix}\begin{Bmatrix} \dot{w}_b \\ \dot{w}_m \\ \dot{w}_\phi \end{Bmatrix} + \left(\lambda \begin{bmatrix} a_a & 0 & 0 \\ 0 & 0 & 0 \\ 0 & 0 & 0 \end{bmatrix} + \begin{bmatrix} k_b & k_{bm} & k_{b\phi} \\ k_{mb} & k_m & k_{m\phi} \\ k_{\phi b} & k_{\phi m} & k_\phi \end{bmatrix} - \begin{bmatrix} k_{N\Delta T} & 0 & 0 \\ 0 & 0 & 0 \\ 0 & 0 & 0 \end{bmatrix} - \begin{bmatrix} k1_{Ne}(w_\phi) & 0 & 0 \\ 0 & 0 & 0 \\ 0 & 0 & 0 \end{bmatrix} + \begin{bmatrix} k2_b(w_b) & 0 & 0 \\ 0 & 0 & 0 \\ 0 & 0 & 0 \end{bmatrix} + \begin{bmatrix} k1_{NB}(w_b) + k1_{Nm}(w_m) & k1_{bm}(w_b) & k1_{b\phi}(w_b) \\ k1_{mb}(w_b) & 0 & 0 \\ k1_{\phi b}(w_b) & 0 & 0 \end{bmatrix} \right) \times \begin{Bmatrix} w_b \\ w_m \\ w_\phi \end{Bmatrix} = \begin{Bmatrix} p_{b\Delta T} \\ p_{m\Delta T} \\ p_\phi \end{Bmatrix} \tag{14}$$

where $[m]$, $[g]$, $[a_a]$, and $[k]$ are the element mass, aerodynamic damping, aerodynamic influence, and linear stiffness matrices, respectively; $[k1]$ and $[k2]$ depend linearly and quadratically on the element displacements respectively; $[k1_{Ne}]$ is the stiffness matrix that linearly depends on the electrical degrees of freedom and becomes a constant matrix when the electric field is known; and $\{p\}$ is the element load vector. All of the element matrices are symmetrical except the aerodynamic influence matrix $[a_a]$, which is skew-symmetric. The detailed derivation and expressions of these element matrices can be found in Ref. 12.

By summing up the contributions from all of the elements and taking account of the kinematic boundary conditions, the system equations of motion for a given rectangular panel can be written into two sets of equations, namely, the actuator equation and the sensor equation.

Actuator equation:

$$(1/\omega_0^2)[M]\{\ddot{W}\} + (g_a/\omega_0)[G]\{\dot{W}\} + (\lambda[A_a] + [K] - [K_{N\Delta T}] - [K1_{Ne}] + [K1] + [K2])\{W\} + ([\Theta]_l + [\Theta]_{nl})\{W_\phi\} = \{P_{\Delta T}\} \tag{15a}$$

Sensor Equation:

$$([\Theta]_l + [\Theta]_{nl})^t\{W\} + [K_\phi]\{W_\phi\} = \{P_\phi\} \tag{15b}$$

where $\{W\} = \{W_b, W_m\}^t, \{W_\phi\} = \{\{w_\phi\}_1, \ldots, \{w_\phi\}_N\}^t$, N is piezoelectric actuator/ sensor sets in the x–y plane, and $[\Theta]_l$ and $[\Theta]_{nl}$ are the linear and nonlinear electromechanical coupling matrices that have the form

$$[\Theta]_l = \begin{bmatrix} K_{b\phi} \\ K_{m\phi} \end{bmatrix} = \left[\sum_{\substack{\text{piezo} \\ \text{elements}}} \begin{bmatrix} [k_{b\phi}] \\ [k_{m\phi}] \end{bmatrix}_1 \cdots \sum_{\substack{\text{piezo} \\ \text{elements}}} \begin{bmatrix} [k_{b\phi}] \\ [k_{m\phi}] \end{bmatrix}_N \right] \tag{16}$$

$$[\Theta]_{nl} = \begin{bmatrix} K1_{b\phi} \\ 0 \end{bmatrix} = \left[\sum_{\substack{\text{piezo} \\ \text{elements}}} \begin{bmatrix} [k1_{b\phi}] \\ 0 \end{bmatrix}_1 \cdots \sum_{\substack{\text{piezo} \\ \text{elements}}} \begin{bmatrix} [k1_{b\phi}] \\ 0 \end{bmatrix}_N \right] \tag{17}$$

Equations (15) represent the general equations of motion for a fluttering composite panel with the thermal and piezoelectric effects. The electrode arrangement and piezoelectric geometry could be arbitrary.

Modal Transformation and Reduction

Unsymmetric Panel

The system equations of motion, Eqs. (15), are not suitable for control design because 1) the order of degrees of freedom of the system displacement vector is too large, and 2) the nonlinear stiffness matrices are functions of system displacement vector. Therefore, these equations have to be transferred into a set of properly chosen modal coordinates with much smaller and manageable degrees of freedom. This is accomplished by a modal transformation[12,13]

$$\{W\} = \sum_{r=1}^{n} q_r(t)\varphi_r = \Psi \boldsymbol{q} \tag{18}$$

where $\boldsymbol{q}$ is the modal coordinate vector, and n is generally less than 10.

With the modal transformation of Eq. (18), the system equations of motion, Eqs. (15), are thus transferred into the reduced modal coordinates as

$$\boldsymbol{M}\frac{\mathrm{d}^2\boldsymbol{q}}{\mathrm{d}\tau^2} + \boldsymbol{C}_d\frac{\mathrm{d}\boldsymbol{q}}{\mathrm{d}\tau} + (\boldsymbol{K} + \boldsymbol{K}_q + \boldsymbol{K}_{qq})\boldsymbol{q} - \boldsymbol{K}_e\boldsymbol{V} = \boldsymbol{F}_s \tag{19a}$$

$$\boldsymbol{K}_e^t\boldsymbol{q} + \boldsymbol{K}_\phi\boldsymbol{V} = \boldsymbol{F}_\phi \tag{19b}$$

where $\tau = \omega_0 t$ is the nondimensional time, and the modal mass $\boldsymbol{M}$ and aerodynamic damping $\boldsymbol{C}_d$ matrices both are diagonal; $\boldsymbol{K}_q$ and $\boldsymbol{K}_{qq}$ are linear and quadratic in terms of the modal coordinate $\boldsymbol{q}$, respectively; $\boldsymbol{K}_\phi$ is the piezoelectric capacitor matrix; and $\boldsymbol{K}_e$ is the electromechanical coupled modal matrix. The terms $\boldsymbol{F}_s$ and $\boldsymbol{F}_\phi$ are the mechanical and electrical modal load vectors, respectively.

Symmetric Panel

Figure 1 shows a typical laminated composite panel containing the embedded piezoelectric layers of equal thickness placed symmetrically with respect to the midplane of the panel. For a symmetrically laminated panel configuration under a steady-state uniform temperature distribution ΔT, the stiffness matrices due to the laminate stiffness $[B]$ and the thermal bending load vector are all null; that is,

$$[K]_{bm} = [K]_{mb} = [K1_{NB}]_b = \{P_{b\Delta T}\} = 0 \tag{20}$$

Then Eqs. (15) can be simplified by neglecting the in-plane inertia and then substituting the in-plane displacement $\{W_m\}$ in terms of transverse displacement $\{W_b\}$. The dynamic equations of motion can be expressed, by collecting the terms, as

$$\left(1/\omega_0^2\right)[M_b]\{\ddot{W}_b\} + (g_a/\omega_0)[G]\{\dot{W}_b\}$$

$$+ ([\bar{K}] + [\overline{K1}] + [\overline{K2}])\{W_b\} + [K_e]\{W_\phi\} = 0 \tag{21a}$$

$$[\bar{K}_e]^t\{W_b\} + [\bar{K}_\phi]\{W_\phi\} = \{\bar{P}_\phi\} \tag{21b}$$

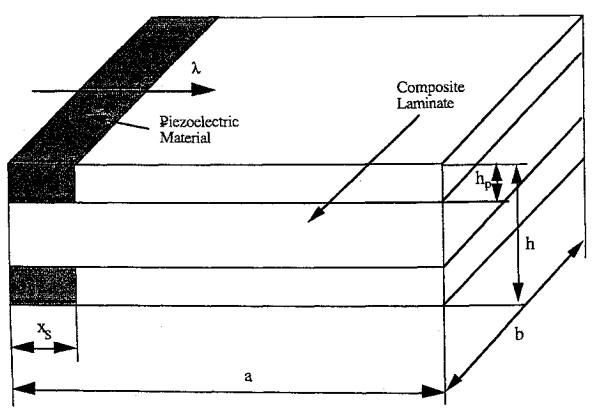

Fig. 1 Configuration of a composite panel with embedded piezoceramics.

where $[M_b]$ and $[G]$ are the panel mass and aerodynamic damping matrices, respectively.

Since the bending φ_{rb} and the membrane φ_{rm} mode shapes in Eq. (18) are uncoupled, a properly chosen modal transformation will have the form[13]

$$\{W_b\} = \sum_{r=1}^{n} q_r(t)\varphi_{rb} = \Psi \boldsymbol{q} \tag{22}$$

The system equations of motion in this symmetric case reduce to

$$\boldsymbol{M}\frac{\mathrm{d}^2\boldsymbol{q}}{\mathrm{d}\tau^2} + \boldsymbol{C}_d\frac{\mathrm{d}\boldsymbol{q}}{\mathrm{d}\tau} + (\boldsymbol{K} + \boldsymbol{K}_{qq})\boldsymbol{q} - \boldsymbol{K}_e\boldsymbol{V} = 0 \tag{23a}$$

$$\bar{\boldsymbol{K}}_e^t\boldsymbol{q} + \bar{\boldsymbol{K}}_\phi\boldsymbol{V} = \boldsymbol{F}_\phi \tag{23b}$$

The detailed expressions for the modal matrices and vector in the preceding equation can be found in Refs. 12 and 13.

The piezoelectric layers (top and bottom) of the present design in Fig. 1 can be stimulated such that one layer contracts, another expands, to create bending moments and in-plane forces if the strains or stresses induced by electric fields in both layers are not balanced. The bending moment has been proved to be more effective to suppress the nonlinear flutter motions than the in-plane force[8]; therefore, only bending moment is considered in the present analysis.

The coupled modal equations of motion for the symmetric case, Eqs. (23), differ from the unsymmetric case, Eqs. (19), not only in their different expressions for the modal matrices, but also in the vanishing of the quadratic nonlinear term $\boldsymbol{K}_q\boldsymbol{q}$ that will normally have the soft spring effect. Furthermore, the right-hand side of Eq. (23a) is zero since no thermal bending moment is created for the symmetric case.

Controller Design

An optimal control approach based on linear optimal control theory[14] is presented. The linear model is obtained by ignoring the nonlinear terms from the modal equations of motion, Eqs. (19), as

$$\boldsymbol{M}\frac{\mathrm{d}^2\boldsymbol{q}}{\mathrm{d}\tau^2} + \boldsymbol{C}_d\frac{\mathrm{d}\boldsymbol{q}}{\mathrm{d}\tau} + \boldsymbol{K}\boldsymbol{q} = \boldsymbol{K}_{el}\boldsymbol{V} + \boldsymbol{F}_s \tag{24a}$$

$$\boldsymbol{K}_{el}^t\boldsymbol{q} + \boldsymbol{K}_\phi\boldsymbol{V} = \boldsymbol{F}_\phi \tag{24b}$$

where the matrix $\boldsymbol{K}_{el}$ is the linear part of the electromechanical coupling matrix

$$\boldsymbol{K}_{el} = -\Psi^t[\Theta]_l \tag{25}$$

The in-plane force induced by piezoelectric materials on nonlinear panel flutter suppression has been dropped in this study. Thus the control variable $\boldsymbol{V}$ induces bending moment only. The equations of motion, Eq. (24a), can be expressed in state space form as

$$\frac{\mathrm{d}\boldsymbol{X}}{\mathrm{d}\tau} = \boldsymbol{A}\boldsymbol{X} + \boldsymbol{B}\boldsymbol{U} \tag{26}$$

where

$$\boldsymbol{X} = \begin{Bmatrix} \boldsymbol{q} \\ \dfrac{\mathrm{d}\boldsymbol{q}}{\mathrm{d}\tau} \end{Bmatrix}, \qquad \boldsymbol{A} = \begin{bmatrix} 0 & \boldsymbol{I} \\ -\boldsymbol{M}^{-1}\boldsymbol{K} & -\boldsymbol{M}^{-1}\boldsymbol{C}_d \end{bmatrix}$$

$$\boldsymbol{B} = \begin{bmatrix} 0 & 0 \\ \boldsymbol{M}^{-1} & \boldsymbol{M}^{-1}\boldsymbol{K}_{el} \end{bmatrix}, \qquad \boldsymbol{U} = \begin{Bmatrix} \boldsymbol{F}_s \\ \boldsymbol{V} \end{Bmatrix}$$

The linear quadratic performance index for optimal control can be formulated as

$$J = \frac{1}{2}\int_0^\infty (\boldsymbol{X}^t\boldsymbol{Q}\boldsymbol{X} + \boldsymbol{U}^t\boldsymbol{R}\boldsymbol{U})\,\mathrm{d}\tau \tag{27}$$

where $\boldsymbol{Q}$ is a positive semidefinite state penalty matrix, and $\boldsymbol{R}$ is a positive definite control penalty matrix. From the optimal control theory, the optimal controller for this linear quadratic regulator problem is

$$\boldsymbol{U} = -\boldsymbol{R}^{-1}\boldsymbol{B}^t\boldsymbol{P}\boldsymbol{X} = -\boldsymbol{k}\boldsymbol{X} \tag{28}$$

where $\boldsymbol{P}$ is a positive definite matrix obtained from the Riccati equation.[14] The feedback control gain from Eq. (28) is defined as

$$\boldsymbol{k} = -\boldsymbol{R}^{-1}\boldsymbol{B}^{t}\boldsymbol{P} \tag{29}$$

The norms of feedback control gain (NFCG) are used to determine the optimal shape and location of piezoelectric actuators, and the NFCG can be defined as

$$\text{NFCG} = \sqrt{\sum_{j=1}^{2n} k_{ij}^2} \qquad (i = 1, 2, \ldots, N) \tag{30}$$

where $2n$ is the total number of state variables defined in Eq. (26) and N is the number of piezoelectric actuator sets.

Results and Discussions

The piezoelectric materials are assumed to behave isotropically and are embedded within the composite panel at top and bottom layers. The C^1 conforming rectangular element is used in the finite element model and the panel is modeled as 10×6 (10 in x and 6 in y direction, total 60 elements) mesh for simply supported condition and 12×6 mesh for clamped condition. The in-plane displacements at the edges are considered to be immovable, i.e., $u = v = 0$ for all boundaries. The panels considered are square or rectangular $[0/45/-45/90]_s$ and $[0/90]$ graphite/epoxy composite. The geometry of the panel is $a = 12$ or 24 (in.), $b = 12$ (in.), $h = 0.05$ (in.), and $h_p = 0.00625$ (in.) (see Fig. 1). The material properties of the composite panel and piezoelectric material are as follows.

Composite lamina:

$$E_1 = 22.5\,\text{Msi}\,(155\,\text{GPa})$$
$$E_2 = 1.17\,\text{Msi}\,(8.07\,\text{GPa})$$
$$G_{12} = 0.66\,\text{Msi}\,(4.55\,\text{GPa})$$
$$\nu_{12} = 0.22$$
$$\alpha_1 = -0.04 \times 10^{-6}/^{\circ}\text{F}\,(-0.07 \times 10^{-6}/^{\circ}\text{C})$$
$$\alpha_2 = 16.7 \times 10^{-6}/^{\circ}\text{F}\,(30.1 \times 10^{-6}/^{\circ}\text{C})$$
$$\rho = 0.1458 \times 10^{-3}\,\text{lb-s}^2/\text{in.}^4\,(1550\,\text{kg/m}^3)$$

Piezoelectric layer (PZT):

$$E = 9.0\,\text{Msi}\,(62.1\text{GPa})$$
$$\nu = 0.3$$
$$\rho = 0.7101 \times 10^{-3}\,\text{lb-s}^2/\text{in.}^4\,(7549\,\text{kg/m}^3)$$
$$\alpha = 3 \times 10^{-6}\,1/^{\circ}\text{F}\,(5.41 \times 10^{-6}/^{\circ}\text{C})$$
$$d_{31} = -7.51 \times 10^{-9}\,\text{in./v}\,(-1.9 \times 10^{-10}\,\text{m/v})$$
$$E_{3\max} = 1.52 \times 10^{4}\,\text{v/in.}\,(6.0 \times 10^{5}\,\text{v/m})$$

Figure 2 shows the convergence of limit-cycle results by retaining different numbers of modes (n) in the modal transformation equation, Eq. (22). It can be seen that a six-mode model will give converged results. Limit-cycle results by Dowell[1] and by finite element frequency domain method[15] using 48 discrete Kirchhoff triangular (DKT) elements (half-plate modeled with $8 \times 3 \times 2$ mesh) are shown in Fig. 3 for comparison. It demonstrates the excellent agreement of three approaches. Thus, six modes are used for all of the simulations. Furthermore, the nonlinear modal equations of motion are used for all of the numerical simulations, and the Runge–Kutta method is used for numerical integration.

Symmetric [0/45/ −45/90]s Panel

A simply supported square $[0/45/-45/90]_s$ graphite/epoxy composite panel (referred as type I panel) is first investigated. The panel becomes less stiff when piezoelectric materials are embedded in, and thus the critical dynamic pressure λ_{cr} is decreased. As the piezoelectric materials replace the top and bottom graphite/epoxy layers completely, the composite panel then becomes $[\text{Piezo}/45/-45/90]_s$ (referred as types II panel). The D_{110} in Eq. (2) for both types of panels are still the same for comparison purpose. The λ_{cr} for types I and II panels are found to be 298 and 227, respectively.

Table 1 Comparison of maximum flutter-free dynamic pressure λ_{max} for one-set actuator placed at the leading edge

x_s/a	$\lambda_{max}(R = 500 \times I)$	$\lambda_{max}(R = 1000 \times I)$
0.0	298(=λ_{cr})	298(=λ_{cr})
0.1	600	616
0.2	819	878
0.3	877	975
0.4	1157	1262
0.5	1100	1171
0.6	1037	1150
1.0	597 ($\lambda_{cr} = 227$)	596 ($\lambda_{cr} = 227$)

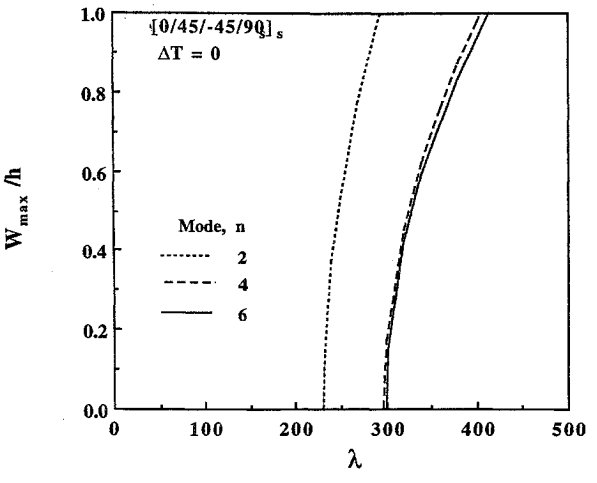

Fig. 2 Convergence of limit-cycle amplitudes for a simply supported square $[0/45/-45/90]_s$ panel ($\mu/M_\infty = 0.01$).

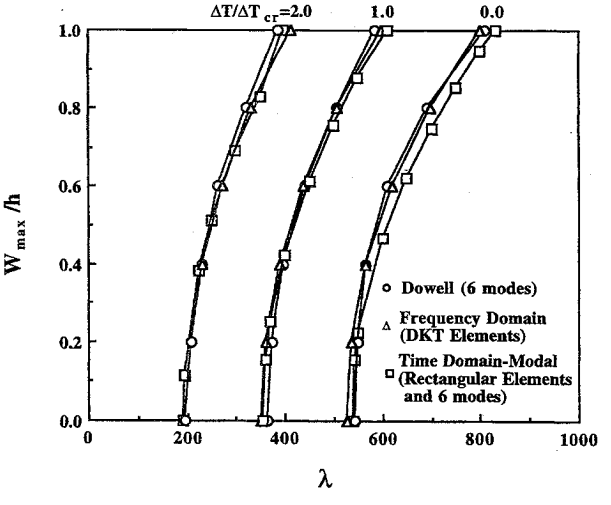

Fig. 3 Comparison of limit-cycle amplitudes for a simply supported square isotropic panel ($\mu/M_\infty = 0.1$).

Table 1 shows the values of λ_{max} for the different sizes of one-set actuator design placed at the leading edge (see Fig. 1) and two constants for $\boldsymbol{R}$ matrix in Eq. (27). For the small-size actuator design ($x_s/a < 0.3$), λ_{max} is low due to the limited moments induced by the piezoelectric material. When piezoelectric layers completely replace the top and bottom layers of the composite laminate ($x_s/a = 1.0$), λ_{max} drops since the panel reduces to type II with smaller critical dynamic pressure. It can be concluded that more piezoelectric materials do not guarantee to have better performance for flutter suppression. The λ_{max} can be increased slightly with larger $\boldsymbol{R}$. The time to suppress the flutter motions, however, will be longer for this case.

For the type II $[\text{Piezo}/45/-45/90]_s$ panel, a two-set piezoelectric actuator design would lead to a better performance than the one-set actuator at the leading edge due to the flexibility of two control variables. The λ_{max} varying with the normalized separating position

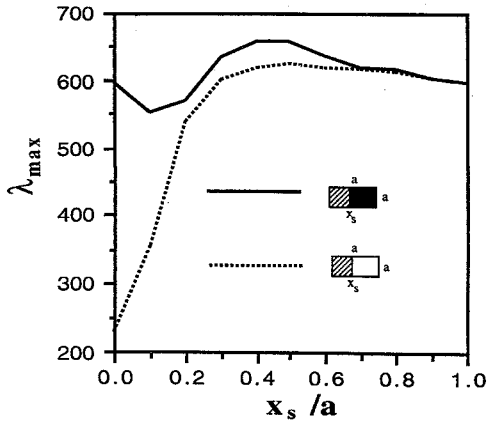

Fig. 4 Maximum flutter-free dynamic pressure vs normalized separating position for a simply supported square [piezo/45/−45/90]$_s$ panel.

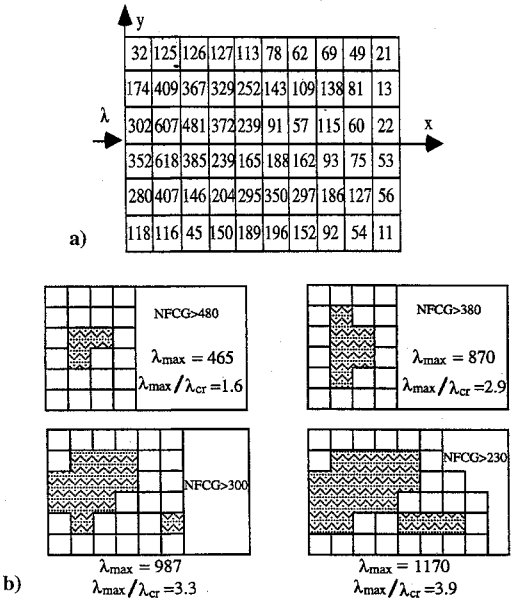

Fig. 5 For a simply supported square [0/45/−45/90]$_s$ panel: a) NFCG and b) optimal location for one-set partially covered piezoelectric actuator.

for one-set (dotted line) and two-set (solid line) actuator designs of this type of panel is shown in Fig. 4 ($\boldsymbol{R} = 500 \times \boldsymbol{I}$). The result clearly shows a better performance for the two-set actuator design. It is also shown that the λ_{max} reaches to its maximum at about x_s/a at half of the panel. The two-set actuator design will increase the critical dynamic pressure about three times ($\lambda_{max}/\lambda_{cr} = 3$) for this type of composite panel.

One of the objectives of this study is to use as little piezoelectric material as possible to achieve a higher λ_{max}. The shape and location of the piezoelectric actuator then become crucial. The type II panel with fully embedded piezoelectric material is first divided into a number of small patches that equal the number of finite elements used. The NFCG values are then calculated for each set at $\lambda = 1000$ and $\boldsymbol{R} = 1000 \times \boldsymbol{I}$ and the result is shown in Fig. 5a. The higher the value is, the more control influence of the corresponding patch is for the flutter control. By connecting these small patches, the optimal shape and location of the actuator can be determined. Figure 5b illustrates four actuator configurations of one-set design based on the NFCG. The size of piezoelectric material is limited to 18 elements for the sake of keeping the panel close to the type I. The critical dynamic pressure λ_{cr} for the type I panel without piezoelectric materials is 298. Table 2 compares the λ_{max} and the ratio of λ_{max} to λ_{cr} for three different sizes of actuators (6,12, and 18 element size) based on two types of designs. The advantage of using the NFCG to design the actuator rather than simply placing the actuator at the

Table 2 Comparison of λ_{max} of two different designs

Actuator at the leading edge			Actuator based on NFCG		
xs/a	λ_{max}	$\lambda_{max}/\lambda_{cr}$	Size	λ_{max}	$\lambda_{max}/\lambda_{cr}$
0.1	616	2.1	6	870	2.9
0.2	878	2.9	12	987	3.3
0.3	975	3.3	18	1170	3.9

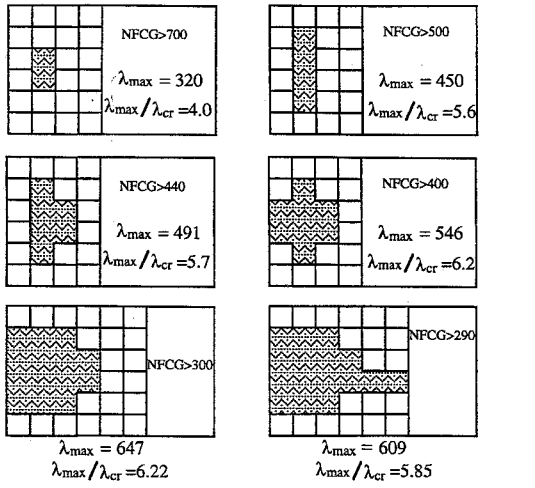

Fig. 6 One-set partially covered piezoelectric actuator designs for a simply supported square [0/90] panel.

leading edge can be clearly seen from the table. For example, the λ_{max} is increased from 616 to 870 when using the NFCG for the equal area of piezoelectric material in both designs. Furthermore, the λ_{max} is increased about four times as compared with that of the panel without piezoelectric actuator. The optimal shape and location for maximizing the dynamic pressure without flutter are thus obtained based upon the NFCG. In the following examples, therefore, the actuators are all designed based on the NFCG criterion.

Unsymmetric [0/90] Panel

A simply supported square unsymmetric [0/90] composite panel is considered as well. The maximum amplitudes of the panel transverse deflection will no longer be symmetric with respect to the midplane of the laminate due to the presence of coupling matrix [B]. The actuator configurations determined based on the NFCG are illustrated in Fig. 6. The maximum flutter-free dynamic pressure λ_{max} is increased first as more piezoelectric materials are added to a certain extent and then drops. Based on the NFCG, the optimal piezoelectric shape and location for suppressing this unsymmetric panel can be determined (300 < NFCG < 400), and the λ_{max} can be increased as high as six times the λ_{cr}.

Aspect Ratio

A simply supported rectangular (aspect ratio $a/b = 2$) [0/45/−45/90]$_s$ composite panel is investigated. The NFCG values are taken at the dynamic pressure equaling 1000 and with the aerodynamic damping of 0.1. The $\boldsymbol{R}$ matrix is $1000 \times \boldsymbol{I}$. Based on the NFCG and λ_{max} values, the optimal designs for the piezoelectric actuators can be found in Fig. 7.

Boundary Conditions

A square [0/45/−45/90]$_s$ composite panel with all edges clamped is investigated. The panel is modeled with 12×6 mesh. Through the study of convergence of critical dynamic pressure, it is found that the six lowest modes (instead of the six modes in x direction used in the simply supported boundary conditions) are suitable for modal reduction in the clamped case. Thus all of the results are obtained based on the modal equations with lowest six modes.

Generally speaking, a clamped panel is much stiffer than the simply supported one and is harder to be controlled. With the same piezoelectric material, the maximum flutter-free dynamic pressure will not be able to increase as much as in the simply supported

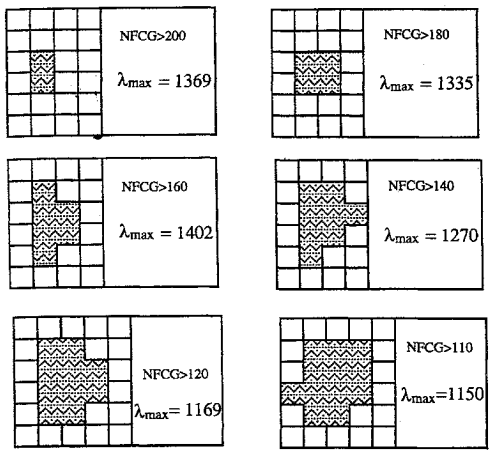

Fig. 7 One-set partially covered piezoelectric actuator designs for a simply supported rectangular $[0/45/-45/90]_s$ panel ($a/b = 2$).

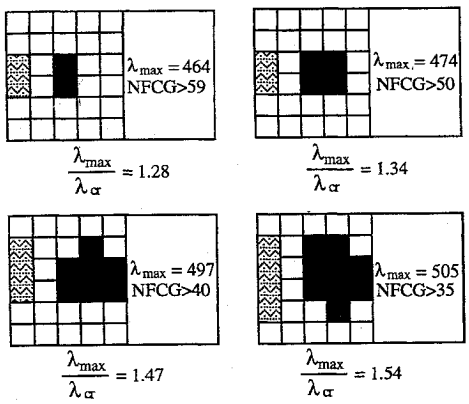

Fig. 8 Two-set partially covered piezoelectric actuator designs for a clamped square $[0/45/-45/90]_s$ panel.

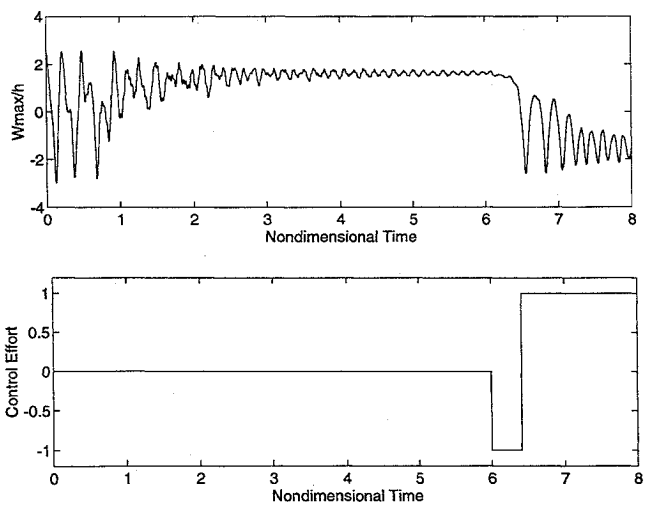

Fig. 9 Thermal buckled deflection and control effort of a simply supported square $[0/45/-45/90]_s$ panel at $\lambda = 100$ and $\Delta T/\Delta T_{cr} = 6.0$.

case. The NFCG values are obtained based on the nondimensional dynamic pressure λ equaling 1000 and the aerodynamic damping 0.1. The $\boldsymbol{R}$ matrix is $1000 \times \boldsymbol{I}$. The NFCG values show that the actuator shapes are not continuous in this case. This suggests us using two-set actuator instead of one-set for clamped square panels. The corresponding configurations for two-set actuator design are given in Fig. 8.

Effect of Temperature

The panel stiffness will tend to reduce with the inclusion of a thermal effect, which would lower the critical dynamic pressure

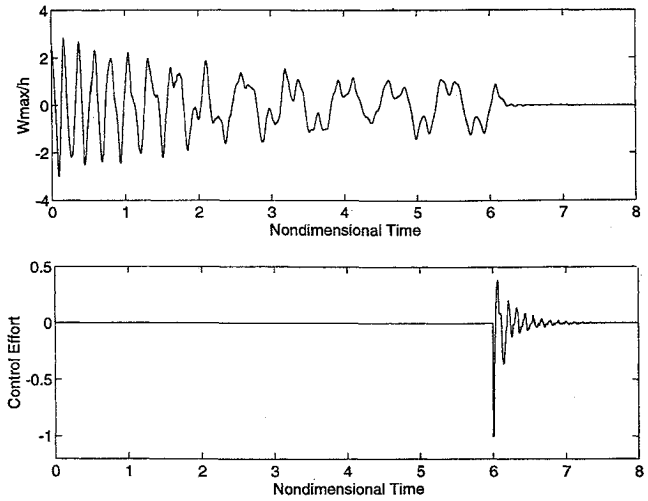

Fig. 10 Control of periodic motion of a simply supported square $[0/45/-45/90]_s$ panel at $\lambda = 140$ and $\Delta T/\Delta T_{cr} = 3.0$.

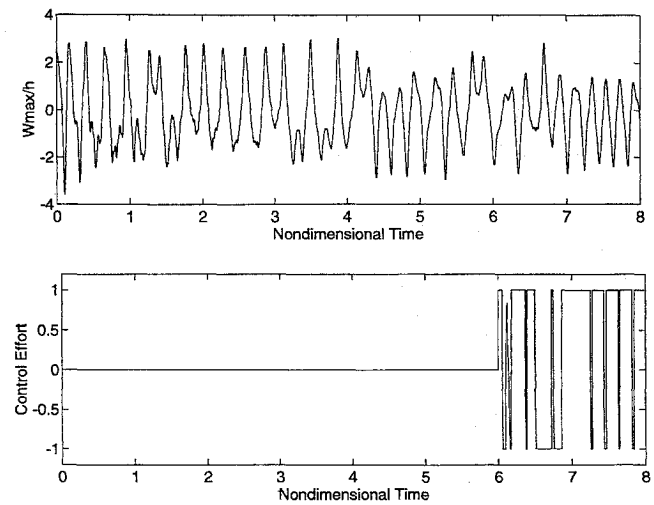

Fig. 11 Control of chaotic motion of a simply supported square $[0/45/-45/90]_s$ panel at $\lambda = 220$ and $\Delta T/\Delta T_{cr} = 6.0$.

(see Fig. 3). This section will address the possibilities of suppressing flutter motions with the effect of uniform temperatures.

A simply supported square $[0/45/-45/90]_s$ composite panel with the inclusion of a piezoelectric actuator is studied based on the configuration (NFCG > 380) shown in Fig. 5b. The critical buckling temperature is found to be $\Delta T_{cr} = 19.7°$F. The flutter suppression is examined under two uniform temperature conditions: moderate temperature ($\Delta T/\Delta T_{cr} = 3.0$) and high temperature ($\Delta T/\Delta T_{cr} = 6.0$). The aerodynamic damping coefficient is 0.01 and the matrix $\boldsymbol{R}$ is $500 \times \boldsymbol{I}$. Once the piezoelectric actuator is actuated, the flutter motions at moderate temperatures and certain dynamic pressures can be suppressed. However, as the temperature increased, the plate deflection will not be able to be suppressed due to the large thermal static deformation of the panel.

Figure 9 shows the panel time history and control effort at a low dynamic pressure ($\lambda = 100$) and high temperature ($\Delta T/\Delta T_{cr} = 6.0$). The thermal shock is clearly demonstrated at the beginning and followed by small oscillations with a constant value that can be considered as a static aerodynamic-thermal buckling deflection. It is shown that the piezoelectric actuator will not be able to suppress the large static aerodynamic-thermal bending of the panel. In Fig. 10, the periodic motions of the panel obtained at the moderate temperature ($\Delta T/\Delta T_{cr} = 3.0$) is shown to be suppressible. The plot is taken at dynamic pressure $\lambda = 140$. Figure 11 illustrates that the panel motion is chaotic at high temperature ($\Delta T/\Delta T_{cr} = 6.0$) and dynamic pressures $\lambda = 220$. With the limited control effort, the panel motion becomes a limit-cycle oscillation. Using an increased piezoelectric

actuation by applying higher maximum electric field (say 80% of the depolarization) with the present actuator configuration or thicker piezoelectric layer, this limit-cycle motion can be suppressed.

Conclusions

A set of coupled structure-electrical nonlinear modal equations are derived for the suppression of flutter motions of composite panels with embedded piezoelectric actuators at supersonic speeds. Only the bending moments induced by the piezoelectric actuators are used to control the panel flutter since the induced in-plane forces are not effective. The linearized modal equations are employed in the linear optimal controller design; however, the nonlinear modal equations are used for flutter suppression simulations.

Two types of actuator designs have been studied: 1) the actuators are placed at the leading edge of the panel, and 2) the actuators are based on the NFCG to determine the shape and location. Both types can be either one set or two set. Examples demonstrate that 1) more piezoelectric material does not always give a larger λ_{max}, 2) the use of NFCG yields better actuator control performance (high λ_{max}), and 3) the two-set actuator design gives better performance than the one-set due to more flexibility in control. The present studies show that the maximum flutter-free dynamic pressure λ_{max} can be increased as high as four to six times the critical dynamic pressure for the simply supported composite panels and only about two times for the clamped panels because the clamped panels are much stiffer.

The high temperature loads can affect flutter response; they may lead to aerodynamic-thermal postbuckling deflection and periodic or chaotic motion.[13,16,17] Examples investigated show that at moderate temperature the panel motion is periodic and the flutter motion can be completely suppressed by the piezoelectric actuation. At high temperature, the panel behavior can be in an aerodynamic-thermal postbuckling or it may have a chaotic motion. With the limited actuator action, the large aerodynamic-thermal deflection is reduced to periodic motions about an equilibrium buckled position and the chaotic motion is reduced to a limit-cycle motion. Both motions, periodic and limit-cycle, can be suppressed if stronger piezoelectric actuation is available. Further investigations on panel flutter in thermal environment are warranted.

References

[1]Dowell, E. H., "Panel Flutter: A Review of the Aeroelastic Stability of Plates and Shells," *AIAA Journal*, Vol. 8, No. 3, 1970, pp. 385–399.

[2]Dowell, E. H., "Nonlinear Oscillations of a Fluttering Plate," *AIAA Journal*, Vol. 4, No. 7, 1966, pp. 1267–1275.

[3]Ashley, H., and Zartarian, G., "Piston Theory—A New Aerodynamic Tool for the Aeroelastician," *Journal of the Aeronautical Science*, Vol. 23, No. 12, 1956, pp. 1109–1118.

[4]Gray, C. E., Jr., and Mei, C., "Large Amplitude Finite Element Flutter Analysis of Composite Panels in Hypersonic Flow," *Proceedings of the AIAA Dynamics Specialist Conference* (Dallas, TX), AIAA, Washington, DC, 1992, pp. 492–512; see also *AIAA Journal*, Vol. 31, No. 6, 1993, pp. 1090–1099.

[5]Zhou, R. C., Xue, D. Y., and Mei, C., "On Analysis of Nonlinear Panel Flutter at Supersonic Speeds," *Proceedings of the First Industry/Academy Symposium on Research for Future Supersonic and Hypersonic Vehicles* (A&T State Univ., Greensboro, NC), TSI Press, Albuquerque, NM, 1994, pp. 343–348.

[6]Scott, R. C., and Weisshaar, T. A., "Controlling Panel Flutter Using Adaptive Materials," *Proceedings of the AIAA/ASME/ASCE/AHS/ASC 32nd Structures, Structural Dynamics, and Materials Conference* (Baltimore, MD), AIAA, Washington, DC, 1991, pp. 2218–2229; see also *Journal of Aircraft*, Vol. 31, No. 1, 1994, pp. 213–222.

[7]Hajela, P., and Glowasky, R., "Application of Piezoelectric Elements in Supersonic Panel Flutter Suppression," AIAA Paper 91-3191, Sept. 1991.

[8]Lai, Z., Xue, D. Y., Huang, J.-K., and Mei, C., "Nonlinear Panel Flutter Suppression with Piezoelectric Actuation," *Journal of Intelligent Material Systems and Structures*, Vol. 6, No. 2, 1995, pp. 274–282.

[9]Xue, D. Y., and Mei, C., "A Study of the Application of Shape Memory Alloy in Panel Flutter Control," *Proceedings of the 5th International Conference on Recent Advances in Structural Dynamics*, Inst. of Sound and Vibration Research, Univ. of Southampton, Southampton, England, UK, 1994, pp. 412–422.

[10]Zhou, R. C., Lai, Z., Xue, D. Y., Huang, J.-K., and Mei, C., "Suppre/-ssion of Nonlinear Panel Flutter at Elevated Temperature with Piezoelectric Actuators," *AIAA Journal*, Vol. 33, No. 6, 1995, pp. 1098–1105.

[11]Crandall, S. H., Karnopp, D. C., Kurtz, E. F., Jr., and Pridmore-Brown, D. C., *Dynamics of Mechanical and Electromechanical Systems*, Krieger, Malabar, FL, 1968.

[12]Zhou, R. C., "Finite Element Analysis for Nonlinear Flutter Suppression of Composite Panels at Elevated Temperatures Using Piezoelectric Materials," Ph.D. Dissertation, Dept. of Aerospace Engineering, Old Dominion Univ., Norfolk, VA, 1994.

[13]Zhou, R. C., Xue, D. Y., and Mei, C., "A Finite Element Time Domain-Modal Formulation for Nonlinear Flutter of Composite Panels at Elevated Temperatures," *AIAA Journal*, Vol. 32, No. 10, 1994, pp. 2044–2052.

[14]Lewis, F. L., *Optimal Control*, Wiley-Interscience, New York, 1986, p. 51.

[15]Xue, D. Y., and Mei, C., "Finite Element Nonlinear Panel Flutter with Arbitrary Temperatures in Supersonic Flow," *AIAA Journal*, Vol. 31, No. 1, 1993, pp. 154–162.

[16]Dowell, E. H., "Flutter of a Buckled Plate as an Example of Chaotic Motion of a Deterministic Autonomous System," *Journal of Sound and Vibration*, Vol. 85, No. 3, 1982, pp. 333–344.

[17]Abbas, J. F., Ibrahim, R. A., and Gibson, R. F., "Nonlinear Flutter of Orthotropic Composite Panel Under Aerodynamic Heating," *AIAA Journal*, Vol. 31, No. 8, 1993, pp. 1478–1488.